Hindawi Publishing Corporation
Journal of Biomedicine and Biotechnology
Volume 2008, Article ID 837653, 9 pages
doi:10.1155/2008/837653

Research Article

Receptor Guided 3D-QSAR: A Useful Approach for Designing of IGF-1R Inhibitors

M. Muddassar, F. A. Pasha, H. W. Chung, K. H. Yoo, C. H. Oh, and S. J. Cho

Future Fusion Technology Division, Computational Science Center, Korea Institute of Science and Technology, P.O. Box 131, Cheongryang, Seoul 130-650, South Korea

Correspondence should be addressed to S. J. Cho, chosj@kist.re.kr

Received 16 August 2007; Accepted 17 December 2007

Recommended by Daniel Howard

Research by other investigators has established that insulin-like growth factor-1 receptor (IGF-1R) is a key oncological target, and that derivatives of 1, 3-disubstituted-imidazo[1,5-α] pyrazine are potent IGF-1R inhibitors. In this paper, we report on our three-dimensional quantitative structure activity relationship (3D-QSAR) studies for this series of compounds. We validated the 3D-QSAR models by the comparison of two major alignment schemes, namely, ligand-based (LB) and receptor-guided (RG) alignment schemes. The latter scheme yielded better 3D-QSAR models for both comparative molecular field analysis (CoMFA) ($q^2 = 0.53$, $r^2 = 0.95$) and comparative molecular similarity indices analysis (CoMSIA) ($q^2 = 0.51$, $r^2 = 0.86$). We submit that this might arise from the more accurate inhibitor alignment that results from using the structural information of the active site. We conclude that the receptor-guided 3D-QSAR may be helpful to design more potent IGF-1R inhibitors, as well as to understand their binding affinity with the receptor.

1. INTRODUCTION

The insulin-like growth factor-1 receptor is a membrane-associated receptor that belongs to subclass I of the receptor tyrosine kinase (RTK) superfamily [1]. IGF-1R has been shown to have significant roles in the regulation of normal cell growth. It has mitogenic and survival effects on human cancer cells [2]. The Binding of IGF-1 to IGF-1R activates the RTK, and later, in turn, activates a cascade of downstream signals, which are postulated to stimulate cell proliferation and enhance resistance to apoptosis [3]. Understandably, the abnormal expression of the IGF-1R has been implicated to cancer. Epidemiological studies have also shown a link between serum concentrations of IGF-1 and IGFBP-3 with increased risks of breast cancer [4]. A number of anticancer agents which inhibit the IGF-1R activity and proliferation [5] have been extracted from plants [6] as well as synthesized, such as BMS-554417 (2-(4-substituted-2-oxo-1,2-dihydropyridin-3-yl)-benzimidazole) [7] and NVP-AEW541 (pyrrolo[2,3-*d*] pyrimidine derivative) molecules. Both of these compounds are orally administered and have proved antitumor activity. Various QSAR techniques are being used to explore more potent ligands [8–11]; but in this study, we performed comparative three-dimensional quantitative structure activity relationship (3D-QSAR) [12–14] analyses on IFG-1R inhibitors [15] of imidazo [1, 5-α] pyrazine derivatives. In 3D-QSAR [14], determination of the bioactive conformer [16] and molecular alignment of the compounds is key factor to get meaningful results. The biologically active conformations of the structures should be aligned in a way that represents a similar binding mode [17]. Here we first applied the ligand-based (LB) strategy using the systematic search-based minimum energy conformer approach [18]. Second, receptor-based 3D-QSAR [19] using molecular docking of inhibitors in the available X-ray crystal structure [20] of the receptor protein. The qualities of these 3D-QSAR models were compared and discussed with respect to the IGF-1R target.

2. MATERIAL AND METHODS

A series of 54 potent 1, 3-disubstituted imidazole [1, 5-α] pyrazine derivatives with their inhibitory activities to IGF-1R were taken from the literature [15]. The dataset was randomly divided into 43 and 11 molecules, the training and test datasets, respectively. The observed IC_{50} values were converted into pIC_{50} values and are reported in Table 1.

Table 1: The structures and observed IGF inhibitory activities [15].

No.	Structure	R	IC_{50} (M)	pIC_{50}
1	A	4-OBn	1.97×10^{-6}	5.706
2	A	3-OH	0.518×10^{-6}	6.286
3	A	3-OBn–4-OMe	1.35×10^{-6}	5.870
4	A	3-OBn–4-OH	3.31×10^{-6}	5.480
5*	B	Cyclopentyl	3.5×10^{-6}	5.456
6	B	Cyclohexyl	1.05×10^{-6}	5.979
7*	B	$-CH_2-$cyclopropyl	2.27×10^{-6}	5.644
8*	B	$-CH_2-$cyclohexyl	1.11×10^{-6}	5.955
9	B	$-CH_2CH_2OMe$	6.28×10^{-6}	5.202
10	B	$-CH_2-$2-pyridyl	1.09×10^{-6}	5.963
11	C	H	0.606×10^{-6}	6.218
12	C	2-F	0.224×10^{-6}	6.650
13	C	3-F	0.51×10^{-6}	6.292
14	C	4-F	1.23×10^{-6}	5.910
15	C	2-Cl	0.343×10^{-6}	6.465
16	C	3-Cl	2.12×10^{-6}	5.674
17*	C	4-Cl	0.980×10^{-6}	6.009
18	C	$2\text{-}OCF_2H$	3.28×10^{-6}	5.484
19	C	$3\text{-}OCF_2H$	5.78×10^{-6}	5.238
20	C	$4\text{-}OCF_2H$	2.82×10^{-6}	5.550
21	C	2,3-Difluoro	0.898×10^{-6}	6.047
22	C	3,4-Difluoro	4.48×10^{-6}	5.349
23*	C	2,5-Difluoro	0.329×10^{-6}	6.483
24	C	2,6-Difluoro	0.215×10^{-6}	6.668
25	C	3,5-Difluoro	1.35×10^{-6}	5.870
26	C	2,6-Dichloro	1.67×10^{-6}	5.777
27	C	2-Cl,6-F	0.248×10^{-6}	6.606
28	D	Cyclopentyl	1.05×10^{-6}	5.979
29	D	Cyclohexyl	3.51×10^{-6}	5.455
30	D	Cycloheptyl	3.79×10^{-6}	5.421
31*	D	Phenyl	1.68×10^{-6}	5.775
32	E	$trans\text{-}NH_2$	0.221×10^{-6}	6.656
33	E	$cis\text{-}NH_2$	0.775×10^{-6}	6.111
34*	E	trans-NHMe	0.105×10^{-6}	6.979
35	E	trans-Pyrrolodinyl	1.82×10^{-6}	5.740
36*	E	trans-Piperidinyl	3.40×10^{-6}	5.469
37	E	trans-NHPh	1.30×10^{-6}	5.886
38	E	trans-NHBn	1.39×10^{-6}	5.857
39	F	$trans\text{-}NH_2$	0.119×10^{-6}	6.924
40	F	$cis\text{-}NH_2$	0.228×10^{-6}	6.642
41	F	$trans\text{-}N(Et)_2$	0.115×10^{-6}	6.939
42	F	trans-Azetidinyl	0.081×10^{-6}	7.092
43	F	trans-Pyrrolidinyl	0.103×10^{-6}	6.987
44*	F	trans-Morpholino	0.091×10^{-6}	7.041
45*	G	trans-Pyrrolidinyl	0.116×10^{-6}	6.936
46	G	cis-Pyrrolidinyl	0.089×10^{-6}	7.051
47	G	$cis\text{-}NH_2$	0.060×10^{-6}	7.222
48	G	$cis\text{-}NMe_2$	0.166×10^{-6}	6.780
49*	G	cis-Piperidinyl	0.237×10^{-6}	6.625
50	G	cis-Morpholino	0.148×10^{-6}	6.830
51	G	cis-NH-iPr	0.220×10^{-6}	6.658
52	G	cis-N(Me)-Piperizinyl	0.265×10^{-6}	6.577

Table 1: Continued.

No.	Structure	R	IC_{50} (M)	pIC_{50}
53	H	trans-NH_2	0.526×10^{-6}	6.279
54	H	cis-NH_2	0.554×10^{-6}	6.256

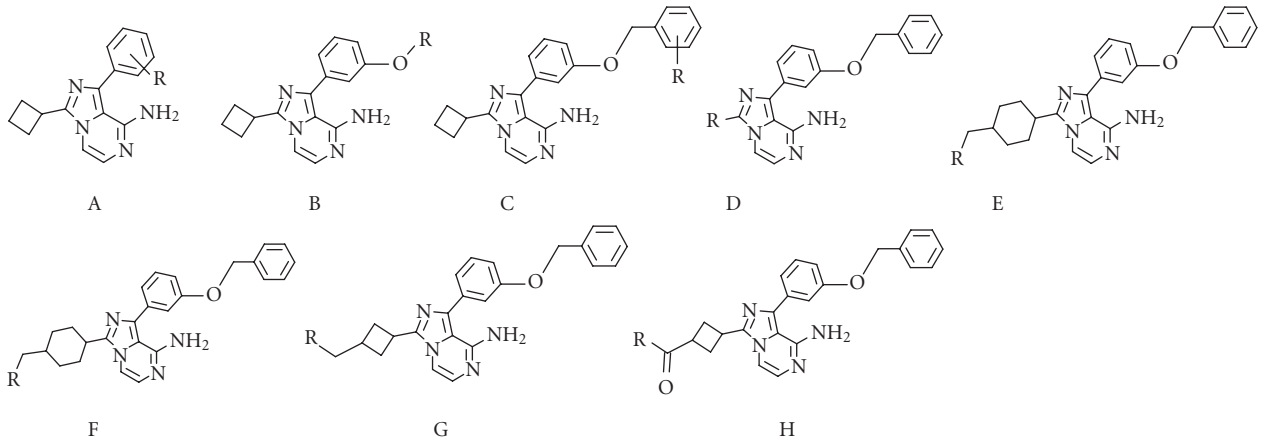

*Compounds used in the test set.

2.1. Computational details

The molecular modeling studies were carried out using SYBYL 7.3. The initial structures were minimized at Tripos force field [21] with MMFF94 charge by using conjugate gradient method, and convergence criterion was 0.005 kcal/mol.The comparative molecular field analysis (CoMFA) and comparative molecular similarity indices analysis (CoMSIA) studies require aligned structures [16]. The ligand-based (LB) and receptor-guided (RG) alignment techniques were used in two geometrical schemes respectively.

2.2. CoMFA and CoMSIA

Lennard-Jones and Coulomb potentials-based CoMFA analysis has been performed and the steric as well as electrostatic energies were calculated by using sp^3 carbon probe atom with Van der Waal radius of 1.52 Å and +1 charge. The energies were truncated to ±30 kcal/mol and the electrostatic contributions were ignored at lattice interactions with maximum steric interactions. The CoMFA were generated by standard method in SYBYL. The CoMSIA models were also derived with the same lattice box used as in CoMFA calculations. All five CoMSIA similarity indices (steric, electrostatic, hydrophobic, H-bond donor, and H-bond acceptor) were evaluated using the probe atom. The CoMSIA models from hydrophobic and H-bonds were calculated between the grid point and each atom of the molecule by a Gaussian function [14]. An attenuation factor's default value of 0.30 was used, which is the standard distance dependence of molecular similarity.

2.3. PLS analysis and validation of QSAR models

In order to derive 3D-QSAR models, the CoMFA and CoMSIA descriptors were used as independent variables and the pIC_{50} values as the dependent variable. Partial least-square (PLS) method [22] was used to linearly correlate these CoMFA and CoMSIA descriptors to the inhibitory activity values. The CoMFA cutoff values were set to 30 kcal/mol for both steric and electrostatic fields, and also all fields were scaled by the default options in SYBYL. The cross-validation analysis was performed using the leave one out (LOO) method in which one compound is removed from the dataset and its activity is predicted using the model derived from the rest of the dataset. The cross-validated correlation coefficient (q^2) that resulted in optimum number of components and lowest standard error of prediction were calculated using the following formulae,

$$q^2 = 1 - \frac{\sum_y (y_{\text{pred}} - y_{\text{observed}})^2}{\sum_y (y_{\text{observed}} - y_{\text{mean}})^2},$$
$$\text{PRESS} = \sum_y (y_{\text{predicted}} - y_{\text{observed}})^2, \quad (1)$$

where y_{pred}, y_{actual}, and y_{mean} are predicted, actual, and mean values of the target property (pIC_{50}), respectively. The non-cross-validated PLS analyses were performed with column filtering value of 2.0, to reduce analysis time with small effect on the q^2 values. To further assess the robustness and statistical confidence of the derived models, bootstrapping analysis for 100 runs were performed.

The predictive power of 3D-QSAR models, derived by using the training set were examined by an external test set of eleven molecules. The predictive ability of the models is expressed by the predictive r^2 value, which is analogous to cross-validated r^2 (q^2) and is calculated using the following formula:

$$r^2_{\text{pred}} = \frac{\text{SD} - \text{PRESS}}{\text{SD}}, \quad (2)$$

where SD is the sum of the squared deviations between the biological activities of the test set and mean activities of the

training molecules and PRESS is the sum of squared deviation between predicted and actual activities of the test set molecules.

3. RESULTS AND DISCUSSION

3.1. Ligand-based alignment

In this scheme, the most active molecule was used as a template. Systematic search routine was used in the conformational analysis and all rotatable bonds were searched in 10° increments from 0° to 350°. Conformational energies were computed with electrostatic term, and the lowest energy conformer was selected. The template was modified for other ligands of the series. All ligands were minimized by Tripos force field but the common moiety was constrained during minimization. The molecules were aligned by superimposing common substructures using SYBYL database alignment option. These aligned structures were subsequently used for ligand-based CoMFA/CoMSIA probe interaction energy calculations.

3.2. Receptor-guided alignment

This geometrical scheme is based on docked geometry. The best docked mode of the smallest compound was taken as template and modified for the other compounds. The compounds were minimized by Tripos force field (Powell method, 2000 iterations, and 0.05 $\text{kcal}\cdot\text{mol}^{-1}\cdot\text{Å}^{-1}$ energy gradient convergence criteria). All minimized structures at this binding mode were superimposed to get the molecular alignment for CoMFA and CoMSIA. The superimposed structures inside the receptor site were further used for CoMFA and CoMSIA analysis.

3.3. Molecular docking

The structure coordinates of IGF-1R were obtained from protein databank (1JQH) [20]. Recently, Mulvihill et al. [15] presented a possible binding mode of compound-2 by using FlexX-based docking. Here we have also performed molecular docking of same compound. The PDB file obtained from protein data bank was used as receptor site. All water molecules were removed and the protein was modified to dock inhibitor. The active site was defined with a distance of 6.5 Å of ATP binding site. The ligand-2 was docked into the monomer unit (A) of IGF-1R and out of 100 conformers the best mode was selected as template. This binding mode seems prominent as the hydrophobic zone of inhibitor corresponds to hydrophobic pocket of IGFR. The residue E-1080, M-1082, K-1033, D-1086, G-1006, and L-1005 makes hinge contact and might have significant role in the inhibition of IGF-1R. It is also clear from all the figures that the depicted mode holds 3 H-bonds in this region. The –OH group of benzene ring makes H-bond with –NH of K-1033, nitrogen of pyrimidine ring makes contact with –NH of M-1082 and both act as H-bond acceptor. The NH_2 group of pyrimidine ring acts as H-bond donor and makes contact with oxygen of E1080.

3.4. CoMFA and CoMSIA results

The CoMFA and CoMSIA studies were carried out by using both geometrical schemes with different descriptors fields independently and in combination. The ligand-based alignment gave better results for CoMFA model using both field descriptors with cross-validated $r^2(q^2) = 0.52$ and non-cross-validated $r^2 = 0.88$, while for CoMSIA model, combination of steric, electrostatic, and H-bond acceptor yielded the best statistical values with $q^2 = 0.42$ and $r^2 = 0.80$. The internal predictivity of these CoMFA and CoMSIA models was also good with boot-strapped correlation coefficient $r^2_{\text{bs}} = 0.91$ and 0.85, respectively. These models were also validated on a test set of 11 molecules with predictive $r^2 = 0.67$ for CoMFA model and 0.57 for CoMSIA model. In comparison to LB, receptor-guided alignment yielded more significant models with better understanding of these inhibitors and receptor interactions. Best CoMFA models were obtained by combination of steric and electrostatic field descriptors with $q^2 = 0.53$ and $r^2 = 0.95$. Whereas steric, electrostatic, and H-bond acceptor filed descriptors gave the best CoMSIA model with $q^2 = 0.51$ and $r^2 = 0.86$. To further asses the robustness and statistical confidence, the boot strapping analysis were performed for 100 runs. The r^2_{bs} for CoMFA = 0.97 and CoMSIA = 0.90 models suggest that a good internal consistency exists within the underlying dataset. The high r^2 predictive values for CoMFA and CoMSIA (0.67 and 0.64, resp.) also prove models validity. In our efforts to obtain the more pronounced model, region focusing was performed. It only yielded high q^2 value which is not sufficient condition for the model to have high predictive power [23]. The regression summary of different 3D-QSAR models obtained at default parameters and after region focusing are presented in Tables 2 and 3, respectively. The predicted pIC_{50} values for training and test set from CoMFA and CoMSIA models are given in Tables 4 and 5, respectively.

In 3D-QSAR, the determination of the bioactive conformer and molecular alignment of the compounds is an important step. In ligand-based techniques, the minimum energy conformers are often used as bioactive conformer. In contrast, the binding poses obtained from cocrystal structure are used in receptor-guided techniques. Here, both techniques were used. The statistical results indicate that conformation obtained from molecular docking is more reliable. In Figure 1, the yellow conformer displays systematic search-based minimum energy conformer while the red structure shows docked conformer. The findings are reasonable as the oxygen attached with benzyl group of docked conformer is more closed to amino acid (Asp1086) that facilitates an H-bonding between –NH of Asp-1086 and this oxygen atom of the inhibitor; but in case of minimum energy conformer (yellow), the benzyl moiety is quite far and disfavors such interactions.

3.5. The CoMFA contour maps

Figures 2 and 3 show the electrostatic and steric contour maps of the best models based on receptor-guided alignment scheme. The electrostatic interactions are represented by

Table 2: Statistical summary of different PLS analysis. (GS: geometrical scheme; SE: standard error of estimate; n.: number of components; F: Fischer's F value for test of significance; r^2_{bs}: coefficient of determination after 100 bootstrapping runs; SD: standard deviation; Field contribution: (S) steric field, (E) electrostatic field, (H) hydrophobic field, (D) H-bond donor field, and (A) H-bond acceptor field.).

Analysis	GS	Field	q^2	n.	r^2	F	SE	r^2_{bs}	SD	r^2_{pred}
CoMFA	LB	S	0.52	4	0.84	50.12	0.23	—	—	—
CoMFA	LB	E	0.38	3	0.73	34.7	0.30	—	—	—
CoMFA	LB	0.49S/0.51E	0.52	4	0.88	70	0.20	0.91	0.1	0.67
CoMFA	RG	S	0.38	4	0.72	24.5	0.31	—	—	—
CoMFA	RG	E	0.42	7	0.86	33.12	0.22	—	—	—
CoMFA	RG	0.45/0.55	0.53	6	0.95	113.6	0.13	0.97	0.00	0.67
CoMSIA	LB	S	0.27	3	—	—	—	—	—	—
CoMSIA	LB	E	0.36	1	—	—	—	—	—	—
CoMSIA	LB	H	0.32	4	—	—	—	—	—	—
CoMSIA	LB	D	0.00	1	—	—	—	—	—	—
CoMSIA	LB	A	0.33	2	—	—	—	—	—	—
CoMSIA	LB	E/S	0.37	2	—	—	—	—	—	—
CoMSIA	LB	0.60E/0.40A	0.41	2	—	—	—	—	—	—
CoMSIA	LB	0.73E/0.27D	0.41	3	—	—	—	—	—	—
CoMSIA	LB	0.51E/.49H	0.39	2	—	—	—	—	—	—
CoMSIA	LB	0.41E/0.27S/0.31A	0.42	4	0.80	39.2	0.26	0.85	0.04	0.57
CoMSIA	LB	E/A/D	0.41	2	—	—	—	—	—	—
CoMSIA	RG	S	0.37	1	—	—	—	—	—	—
CoMSIA	RG	E	0.46	4	—	—	—	—	—	—
CoMSIA	RG	H	0.35	3	—	—	—	—	—	—
CoMSIA	RG	D	0.15	5	—	—	—	—	—	—
CoMSIA	RG	A	0.39	3	—	—	—	—	—	—
CoMSIA	RG	0.71E/0.29S	0.46	5	—	—	—	—	—	—
CoMSIA	RG	0.66E/0.34A	0.52	5	0.85	41.2	0.23	0.89	0.04	0.57
CoMSIA	RG	E/D	0.48	6	—	—	—	—	—	—
CoMSIA	RG	0.57E/0.43H	0.48	5	—	—	—	—	—	—
CoMSIA	RG	0.54E/0.21S/0.25A	0.51	5	0.86	45.4	0.22	0.9	0.03	0.64
CoMSIA	RG	E/A/D	0.47	6	—	—	—	—	—	—

Table 3: Statistics of different PLS analysis after region focusing. (GS: geometrical scheme; SE: standard error of estimate; n.: number of components; F: Fischer's F value for test of significance; r^2_{bs}: coefficient of determination after 100 bootstrapping runs; SD: standard deviation; Field contribution: (S) steric field, (E) electrostatic field, (H) hydrophobic field, (D) H-bond donor field, and (A) H-bond acceptor field.).

Analysis	GS	Field	Grid spacing	q^2	n.	r^2	F	SE	r^2_{bs}	SD	r^2_{pred}
CoMFA	LB	S	0.5 Å	0.59	5	0.84	40.41	0.234	0.89	0.11	0.65
CoMFA	LB	E	0.5 Å	0.13	2	—	—	—	—	—	—
CoMFA	LB	0.57S/0.43E	0.5 Å	0.56	4	0.84	49.62	0.235	076	0.13	0.68
CoMFA	LB	S	1.5 Å	0.25	1	0.36	23.40	0.450	—	—	—
CoMFA	LB	E	1.5 Å	−0.03	1	—	—	—	—	—	—
CoMFA	LB	0.35S/0.65E	1.5 Å	0.38	2	0.51	21.20	0.40	—	—	—
CoMFA	RG	S	0.5 Å	0.41	4	0.71	23.47	0.315	—	—	—
CoMFA	RG	E	0.5 Å	0.42	7	0.87	33.11	0.220	—	—	—
CoMFA	RG	0.47S/0.53E	0.5 Å	0.55	6	0.94	97.78	0.145	0.96	0.02	0.67
CoMFA	RG	S	1.5 Å	0.44	4	0.65	17.93	0.345	—	—	—
CoMFA	RG	E	1.5 Å	0.11	4	0.26	3.32	0.505	—	—	—
CoMFA	RG	0.45S/0.50E	1.5 Å	0.29	3	0.60	18.99	0.370	—	—	—

Table 4: Experimental and predicted activities with their residuals by CoMFA and CoMSIA analyses of the training set.

n.	CoMFA			CoMSIA	
	Experimental	Predicted		Predicted	
	pIC_{50}	pIC_{50}	Residual	pIC_{50}	Residual
1	5.706	5.553	0.153	5.646	0.060
2	6.286	6.296	−0.010	6.172	0.114
3	5.870	5.948	−0.078	5.781	0.089
4	5.480	5.888	−0.408	5.814	−0.334
6	5.979	5.365	0.614	5.421	0.558
9	5.202	5.275	−0.073	5.074	0.128
10	5.963	6.200	−0.237	6.199	−0.236
11	6.218	6.191	0.027	6.135	0.083
12	6.650	6.276	0.374	6.330	0.320
13	6.292	6.065	0.227	5.849	0.443
14	5.910	5.870	0.040	5.842	0.068
15	6.465	6.487	−0.022	6.363	0.102
16	5.674	5.927	−0.253	5.787	−0.113
18	5.484	5.473	0.011	5.589	−0.105
19	5.238	5.102	0.136	5.579	−0.341
20	5.550	5.615	−0.065	5.625	−0.075
21	6.047	6.015	0.032	6.226	−0.179
22	5.349	5.544	−0.195	5.754	−0.405
24	6.668	6.571	0.097	6.474	0.194
25	5.870	6.034	−0.164	5.832	0.038
26	5.777	5.929	−0.152	6.416	−0.639
27	6.606	6.586	0.02	6.498	0.108
28	5.979	5.981	−0.002	5.676	0.303
29	5.455	5.471	−0.016	5.562	−0.107
30	5.421	5.473	−0.052	5.604	−0.183
32	6.656	6.366	0.290	6.297	0.359
33	6.111	6.366	−0.255	6.297	−0.186
35	5.740	5.706	0.034	6.068	−0.328
37	5.886	5.934	−0.048	5.864	0.022
38	5.857	5.828	0.029	5.763	0.094
39	6.924	6.826	0.098	6.785	0.139
40	6.642	6.826	−0.184	6.785	−0.143
41	6.939	7.009	−0.070	6.951	−0.012
42	7.092	7.032	0.060	6.916	0.176
43	6.987	7.012	−0.025	7.008	−0.021
46	7.051	6.950	0.101	7.130	−0.079
47	7.222	7.325	−0.103	7.126	0.096
48	6.780	6.763	0.017	6.881	−0.101
50	6.830	6.776	0.054	6.842	−0.012
51	6.658	6.648	0.010	6.806	−0.148
52	6.577	6.547	0.030	6.429	0.148
53	6.279	6.328	−0.049	6.298	−0.019
54	6.256	6.328	−0.072	6.298	−0.042

Table 5: Experimental and predicted activities with their residuals by CoMFA and CoMSIA analyses of the test set.

n.	CoMFA			CoMSIA	
	Experimental pIC_{50}	Predicted pIC_{50}	Residual	Predicted pIC_{50}	Residual
5	5.456	5.404	0.052	5.536	−0.080
7	5.644	5.779	−0.135	5.811	−0.167
8	5.955	6.015	−0.060	5.787	0.168
17	6.009	5.966	0.043	5.819	0.190
23	6.483	6.274	0.209	6.304	0.179
31	5.775	5.703	0.072	5.728	0.047
34	6.979	6.269	0.710	6.205	0.774
36	5.469	5.696	−0.227	5.924	−0.455
44	7.041	7.080	−0.039	7.227	−0.186
45	6.936	6.950	−0.014	7.130	−0.194
49	6.625	6.902	−0.277	6.834	−0.209

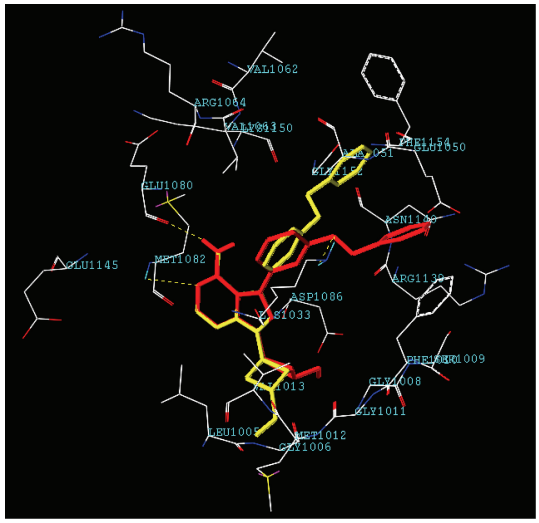

Figure 1: Comparison of minimum energy (yellow) and docking based (red) conformers.

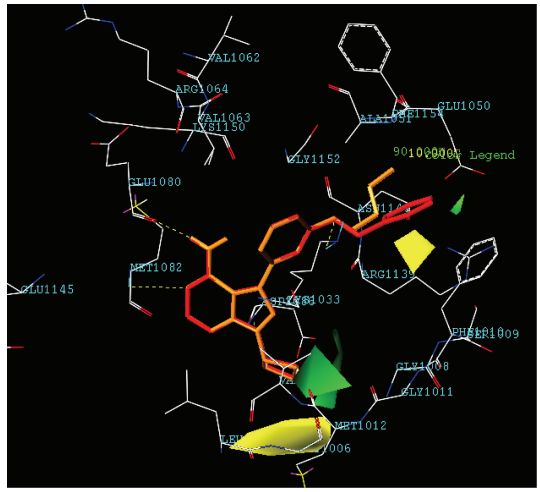

Figure 3: CoMFA steric maps with the most (red) and least (orange) active compound within the active site.

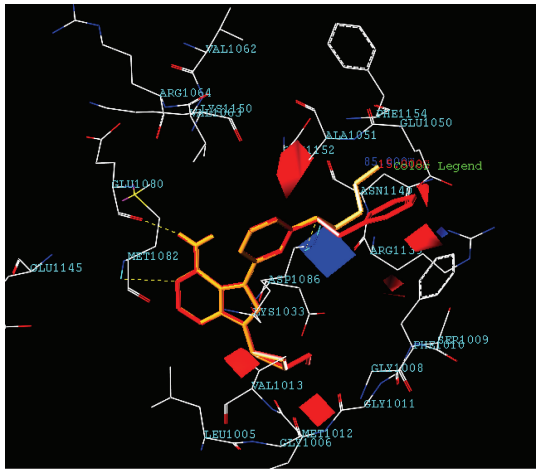

Figure 2: CoMFA electrostatic maps with the most (red) and least (orange) active compound within the active site.

red- and blue-colored contours while steric interactions are represented by green and yellow colored contours. In electrostatic field, blue color contour represents region where electropositive group enhances the activity, whereas red-color region likes electron-rich groups to increase the biological activity. In case of steric interactions, the green region demands bulky substituents to enhance the activity, while in yellow contours, bulky substituents decrease the activity.

The most potent compound-47 (red color) and least-active compound-9 (orange color) of the series with CoMFA contour maps have been superimposed in the active site of the receptor protein. Figure 2 shows that red polyhedrons locate the region where electron-rich group will enhance the inhibitory activity, and vice versa for blue polyhedron. Therefore, the phenyl ring in compound-47 might be responsible for its higher activity than methoxy group of compound-9 because it might have the π-π interactions with the phenyl ring of phenyl alanine (Phe1010) amino acid. The

red contour around 1–3 carbon of cyclobutane also demands the electron-rich group for higher potency. Compound-47 has amino group at C-3 position which might be responsible for its higher activity than least-active compound-9. It is also clear in most of compounds from the dataset that electron-rich group at this position have higher activity than compound-9. In Figure 3, green polyhedron locates the region where bulky substitutent would increase the inhibitory activity and yellow polyhedron where the steric bulk is not required for high potency of the compounds. The small green contour near the phenyl ring of compound-47 explains its higher activity than compound-9. Similarly, the green contour around 2 and 3 carbon of cyclobutane requires the bulky substitutent to be highly active. Thus the bulky substitutent at this position in dataset favors the higher inhibitory activity of the compounds than compound-9. Yellow polyhedron below the plane of phenyl ring and cyclopropane requires the small group to be more active.

3.6. *CoMSIA contour maps*

The CoMSIA contour maps were also developed on the models based on the geometrical scheme 2. Figures 4, 5, and 6 show the steric electrostatic and H-bond acceptor contour maps superimposed in the active site of the IGF-1R. In CoMSIA method, steric and electrostatic contours maps have the same meaning as that of CoMFA contour maps whereas H-bond acceptor contours are represented by magenta and red colors. Magenta favors H-bond acceptor group while red disfavors. The steric and electrostatic maps are more or less similar to the corresponding CoMFA models (Figures 2 and 3, resp.) except that there is a small green contour near phenyl ring of compound-47 in CoMFA model. In Figure 6, the magenta contour around C-2 and C-3 position of cyclobutane favors the H-bond accepting group to enhance the inhibitory activity of the molecules. Thus the H-bond accepting substituent at C-4 position might enhance inhibitory activity of the compounds through H-bonding with Glycine (Gly1008) or Valine (Val1013).

4. CONCLUSION

A comparative CoMFA and CoMSIA models were developed for the series of potent IGF-1R inhibitors. Ligand-based and receptor-guided protocols were applied to develop the models. Receptor-guided alignment gave models with better statistics than the ones from the ligand-based approach, presumably because the alignment using receptor information is more realistic. Moreover, the interpretation of receptor-guided models are directly associated with the receptor information. That is, in general, the superposition of a CoMFA or CoMSIA contour map inside the receptor shows reasonable correspondence between the contour map property and the physical property of surrounding active site region. This provides more detailed understanding about the interaction between the series of inhibitors and IGF-1R. The information drawn here can be used to design new inhibitors of IGF-1R.

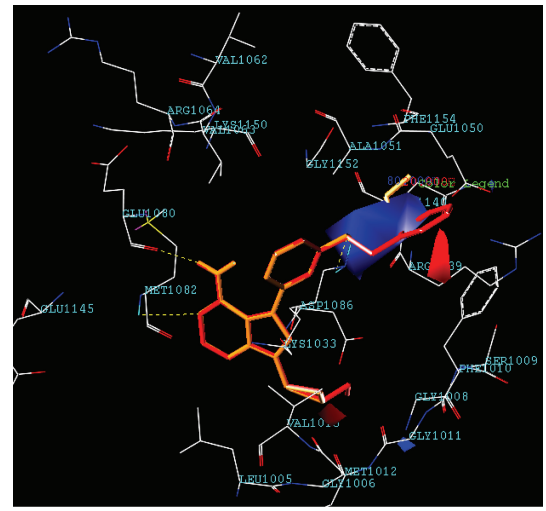

Figure 4: CoMSIA electrostatic maps with the most (red) and least (orange) active compound within the active site.

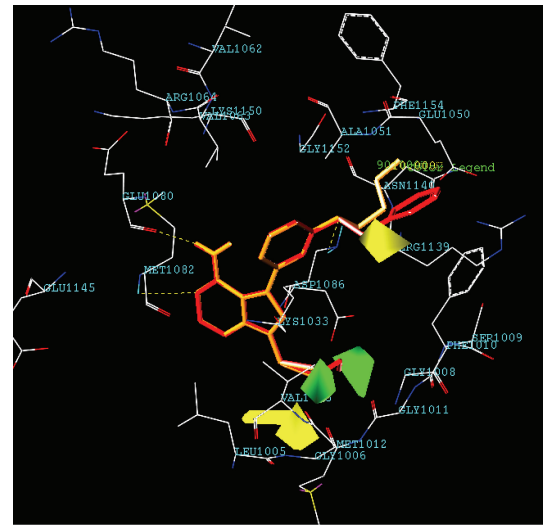

Figure 5: CoMSIA steric maps with the most (red) and least (orange) active compound within the active site.

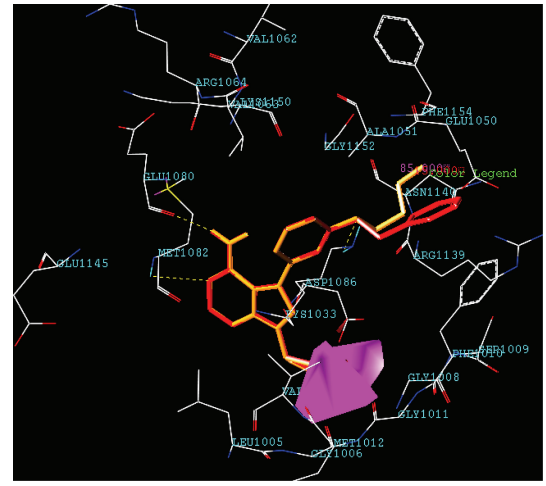

Figure 6: CoMSIA H-bond acceptor map with the most (red) and least (orange) active compound within the active site.

ACKNOWLEDGMENT

The authors would like to thank Jung Soo Oh for the valuable support.

REFERENCES

[1] V. M. Macaulay, "Insulin-like growth-factors and cancer," *British Journal of Cancer*, vol. 65, no. 3, pp. 311–320, 1992.

[2] C. L. Arteaga and C. K. Osborne, "Growth inhibition of human breast cancer cells in vitro with an antibody against the type-I somatomedin receptor," *Cancer Research*, vol. 49, no. 22, pp. 6237–6241, 1989.

[3] H. Werner and D. Le Roith, "New concepts in regulation and function of the insulin-like growth factors: implications for understanding normal growth and neoplasia," *Cellular and Molecular Life Sciences*, vol. 57, no. 6, pp. 932–942, 2000.

[4] S. E. Hankinson, W. C. Willett, G. A. Colditz, et al., "Circulating concentrations of insulin-like growth factor-I and risk of breast cancer," *Lancet*, vol. 351, no. 9113, pp. 1393–1396, 1998.

[5] C. García-Echeverría, M. A. Pearson, A. Marti, et al., "In vivo antitumor activity of NVP-AEW541—a novel, potent, and selective inhibitor of the IGF-IR kinase," *Cancer Cell*, vol. 5, no. 3, pp. 231–239, 2004.

[6] R. Kuttan, P. Bhanumathy, K. Nirmala, and M. C. George, "Potential anticancer activity of turmeric (Curcuma longa)," *Cancer Letters*, vol. 29, no. 2, pp. 197–202, 1985.

[7] P. Haluska, J. M. Carboni, D. A. Loegering, et al., "In vitro and in vivo antitumor effects of the dual insulin-like growth factor-I/insulin receptor inhibitor, BMS-554417," *Cancer Research*, vol. 66, no. 1, pp. 362–371, 2006.

[8] F. A. Pasha, H. W. Chung, S. J. Cho, and S. B. Kang, "3D-quantitative structure activity analysis and quantum chemical analysis of pyrido-di-indoles," *International Journal of Quantum Chemistry*, vol. 108, no. 2, pp. 391–400, 2008.

[9] F. A. Pasha, K. Dal Nam, and S. J. Cho, "CoMFA based quantitative structure toxicity relationship of azo dyes," *Molecular & Cellular Toxicology*, vol. 3, no. 2, pp. 145–149, 2007.

[10] F. A. Pasha, M. M. Neaz, S. J. Cho, and S. B. Kang, "Quantitative structure activity relationship (QSAR) study of estrogen derivatives based on descriptors of energy and softness," *Chemical Biology & Drug Design*, vol. 70, no. 6, pp. 520–529, 2007.

[11] F. A. Pasha, H. K. Srivastava, A. Srivastava, and P. P. Singh, "QSTR study of small organic molecules against Tetrahymena pyriformis," *QSAR and Combinatorial Science*, vol. 26, no. 1, pp. 69–84, 2007.

[12] G. Klebe, U. Abraham, and T. Mietzner, "Molecular similarity indexes in a comparative-analysis (Comsia) of drug molecules to correlate and predict their biological-activity," *Journal of Medicinal Chemistry*, vol. 37, no. 24, pp. 4130–4146, 1994.

[13] G. Klebe, U. Abraham, and T. Mietzner, "Molecular similarity indices in a comparative analysis (CoMSIA) of drug molecules to correlate and predict their biological activity," *Journal of Medicinal Chemistry*, vol. 37, no. 24, pp. 4130–4146, 1994.

[14] R. D. Cramer, D. E. Patterson, and J. D. Bunce, "Comparative molecular field analysis (CoMFA). 1. Effect of shape on binding of steroids to carrier proteins," *Journal of the American Chemical Society*, vol. 110, no. 18, pp. 5959–5967, 1988.

[15] M. J. Mulvihill, Q. S. Ji, D. Werner, et al., "1,3-disubstituted-imidazo[1,5-a]pyrazines as insulin-like growth-factor-I receptor (IGF-IR) inhibitors," *Bioorganic and Medicinal Chemistry Letters*, vol. 17, no. 4, pp. 1091–1097, 2007.

[16] K. H. Kim, G. Greco, and E. Novellino, "A critical review of recent CoMFA applications," *Perspectives in Drug Discovery and Design*, vol. 12–14, pp. 257–315, 1998.

[17] C. Kunick, K. Lauenroth, K. Wieking, et al., "Evaluation and comparison of 3D-QSAR CoMSIA models for CDK1, CDK5, and GSK-3 inhibition by paullones," *Journal of Medicinal Chemistry*, vol. 47, no. 1, pp. 22–36, 2004.

[18] D. C. Juvale, V. V. Kulkarni, H. S. Deokar, N. K. Wagh, S. B. Padhye, and V. M. Kulkarni, "3D-QSAR of histone deacetylase inhibitors: hydroxamate analogues," *Organic and Biomolecular Chemistry*, vol. 4, no. 15, pp. 2858–2868, 2006.

[19] W. Sippl, "Receptor-based 3D QSAR analysis of estrogen receptor ligands—merging the accuracy of receptor-based alignments with the computational efficiency of ligand-based methods," *Journal of Computer-Aided Molecular Design*, vol. 14, no. 6, pp. 559–572, 2000.

[20] A. Pautsch, A. Zoephel, H. Ahorn, W. Spevak, R. Hauptmann, and H. Nar, "Crystal structure of bisphosphorylated IGF-1 receptor kinase: insight into domain movements upon kinase activation," *Structure*, vol. 9, no. 10, pp. 955–965, 2001.

[21] M. Clark, R. D. Cramer, and N. Vanopdenbosch, "Validation of the general-purpose tripos 5.2 force-field," *Journal of Computational Chemistry*, vol. 10, no. 8, pp. 982–1012, 1989.

[22] S. Wold, A. Ruhe, H. Wold, and W. J. Dunn, "The collinearity problem in linear-regression—the partial least-squares (Pls) approach to generalized inverses," *SIAM Journal on Scientific and Statistical Computing*, vol. 5, no. 3, pp. 735–743, 1984.

[23] A. Golbraikh and A. Tropsha, "Beware of q2!," *Journal of Molecular Graphics and Modelling*, vol. 20, no. 4, pp. 269–276, 2002.